



1 **Assessing the influence of soil freeze-thaw cycles on catchment water storage – flux – age interactions**
2 **using a tracer-aided ecohydrological model**

3 Aaron A. Smith¹, Doerthe Tetzlaff^{1,2,3}, Hjalmar Laudon⁴, Marco Maneta⁵, Chris Soulsby³

4 ¹IGB Leibniz Institute of Freshwater Ecology and Inland Fisheries Berlin, Berlin, Germany

5 ²Humboldt University Berlin, Berlin, Germany

6 ³Northern Rivers Institute, School of Geosciences, University of Aberdeen, UK

7 ⁴Department of Forest Ecology and Management, Swedish University of Agricultural Sciences, Umeå, Sweden

8 ⁵Geosciences Department, University of Montana, Missoula, MT

9

10 **Correspondence:** Aaron Smith (smith@igb-berlin.de)

11

12 **Abstract**

13 Ecohydrological models are powerful tools to quantify the effects that independent fluxes may have on catchment storage
14 dynamics. Here, we adapted the tracer-aided ecohydrological model, EcH₂O-iso, for cold regions with the explicit
15 conceptualisation of dynamic soil freeze-thaw processes. We tested the model at the data-rich Krycklan site in northern Sweden
16 with multi-criteria calibration using discharge, stream isotopes and soil moisture in 3 nested catchments. We utilized the model's
17 incorporation of ecohydrological partitioning to evaluate the effect of soil frost on evaporation and transpiration water ages, and
18 thereby the age of source waters. The simulation of stream discharge, isotopes, and soil moisture variability captured the seasonal
19 dynamics at all three stream sites and both soil sites, with notable reductions in discharge and soil moisture during the winter
20 months due to the development of the frost front. Stream isotope simulations reproduced the response to the isotopically-depleted
21 pulse of spring snowmelt. The soil frost dynamics adequately captured the spatial differences in the freezing-front throughout the
22 winter period, despite no direct calibration of soil frost to measured soil temperature. The simulated soil frost indicated a maximum
23 freeze-depth of 0.25 m below forest vegetation. Water ages of evaporation and transpiration reflect the influence of snowmelt-
24 inputs, with a high proclivity of old water (pre-winter storage) at the beginning of the growing season and a mix of snowmelt and
25 precipitation (young water) toward the end of the summer. Soil frost had an early season influence of the transpiration water ages,
26 with water pre-dating the snowpack mainly sustaining vegetation at the start of the growing season. Given the long-term expected
27 change in the energy-balance of northern climates, the approach presented provides a framework for quantifying the interactions
28 of ecohydrological fluxes and waters stored in the soil and understanding how these may be impacted in future.

29 **1. Introduction**

30 Northern watersheds are sensitive hydrologic sites where a significant proportion of the annual water balance is controlled
31 by the spring melt period (Kundzewicz et al., 2007) and can thus be key sentinels for detecting climate change impacts (Woo,
32 2013). Recent data and long-term climate projections indicate a significant increase in warming for extensive areas of boreal forests
33 currently experiencing low-energy, low-precipitation hydroclimatic regimes (Pearson et al., 2013). The implications of the
34 anticipated hydrological change in these catchments for water resources and freshwater ecosystems raise substantial concerns,
35 particularly given the limited number of long-term monitoring sites with high-quality data (Laudon et al., 2018; Tetzlaff et al.,
36 2015). Within changing northern catchments, with high water loss due to transpiration ($\sim 48 \pm 13\%$) (Schlesinger and Jasechko,
37 2014), and significant influence of evapotranspiration (*ET*) fluxes on streamflow (Karlsen et al., 2016a), the long-term
38 ecohydrological implications of vegetation adaptation, plant water use, and the water sources that sustain growth are crucial to



39 understand and quantify. Vegetation in boreal regions also exerts strong influences on the energy balance of such catchments, with
40 low leaf area index (LAI) conifer forests and shrubs affecting the surface albedo, snow interception and affecting the timing and
41 duration of the largest input fluxes of water during snowmelt (Gray and Male, 1981). However, the interactions between soil water
42 storage and “green water” fluxes of transpiration and evaporation are poorly constrained in northern regions, and the way in which
43 sources of water from inputs of snowmelt and summer rainfall mix and sustain plant growth is only just beginning to be understood
44 (Sprenger et al., 2018a). Assessment of these interactions in northern catchments is further complicated by large temperature
45 variations, and the resulting stagnation of hydrological processes induced by frequent frozen ground conditions. With increasing
46 temperatures and potential changes to the winter soil freeze-thaw dynamics (e.g. Venäläinen et al., 2001), it is important to establish
47 how these affect current vegetation-soil water interactions to project the implications of future change.

48 The intricate complexities of changes in the land surface energy balance, temporal changes in sub-surface storage due to frost
49 conditions, and vegetation and soil water usage (transpiration and soil evaporation, respectively), are notoriously challenging to
50 continuously monitor (Maxwell et al., 2019), particularly in northern environments, where site access is typically remote and
51 extreme cold can limit in-situ monitoring devices. In these circumstances, the fusion of sparsely available data with hydrological
52 models is an effective method to quantify water fluxes and storage dynamics at different temporal and spatial scales. While the
53 calibration of such models requires significant hydrometric data inputs, recent work has shown that incorporation of stable isotopes
54 can be an effective tool for constraining the model estimations of storage – flux interactions in the absence of direct in-situ
55 measurements. Such models include (but are not limited to); the STARR (Spatially distributed Tracer-Aided Rainfall-Runoff)
56 model (van Huijgevoort et al., 2016), which was developed for tracer-aided simulations and calibration, and adapted for additional
57 cold-regions processes (Ala Aho et al., 2017a and b; Piovano et al., 2018), CRHM (Cold Regions Hydrologic Model) specific for
58 cold regions (Pomeroy et al., 2007), but not currently using tracers, the isoWATFLOOD model (Stadnyk et al., 2013), which has
59 been used to isolate water fluxes with tracer-aided modelling in large-scale applications in northern regions of Canada, and the
60 EcH₂O-iso model (Maneta and Silverman, 2013; Kuppel et al., 2018 a and b), which was developed as a process-based, coupled
61 atmosphere-vegetation-soil energy balance ecohydrologic model, and modified to incorporate isotopic tracers (stable isotopes
62 deuterium and oxygen-18, $\delta^2\text{H}$ and $\delta^{18}\text{O}$, respectively). However, apart from EcH₂O-iso, which explicitly conceptualises short-
63 term (diurnal and seasonal) and long-term (growth-related) vegetation dynamics and biomass productivity, most of these existing
64 models were mainly developed with a focus on runoff generation (“blue water” fluxes). Consequently, they have very simplistic
65 representation of vegetation – soil – water interactions, estimating *ET* by approximating the physical transpiration controls of
66 vegetation (e.g. Penman-Monteith and Priestley-Taylor methods) and partitioning fluxes after estimation of actual *ET* (Fatichi et
67 al., 2016).

68 Currently, EcH₂O-iso, already incorporates some cold region processes, namely snowpack development, a snowmelt routine,
69 and the influence of temperature effects on vegetation productivity. While the depth of the snowpack is not directly estimated (only
70 snow water equivalent is tracked), the surface energy balance incorporates snowpack heat storage to estimate the warming phase
71 with effective snowmelt timing (Maneta and Silverman, 2013). The model additionally estimates the soil temperatures through
72 multiple soil depths, however, freezing temperature and soil frost development are adaptations that are needed for use in catchments
73 with extensive freezing conditions. Soil freeze-thaw has the potential to significantly influence soil moisture conditions, tracer
74 dynamics, and the magnitude and ages of all water fluxes. The incorporation of tracer dynamics to EcH₂O-iso open opportunities
75 to strengthen the evaluation of the model processes (Kuppel et al., 2018b) and permits the use of tracers in calibration (Douinot et
76 al., submitted). Here, our overall aim was to provide a framework for assessing vegetation influences on the hydrology of cold-
77 regions by adapting the EcH₂O-iso model and testing it in the intensively monitored Krycklan catchment in northern Sweden. The
78 specific objectives of the study are three-fold; 1) to assess the capability of a spatially distributed, physically-based ecohydrological



79 model to capture the influence of snow and soil freeze-thaw processes on water storage dynamics, and the resulting flux magnitudes
80 under different vegetation communities (forest vs mire). 2) To examine the influence of soil frost on the dynamics and age of water
81 fluxes within the catchment, and 3) provide a generic modelling approach for application to other frost affected catchments. In the
82 adaptation of EcH₂O-iso to cold regions and the assessment of the simulated vegetation-soil water interactions with frost
83 conditions, we aim to improve the understanding and projecting the future role of vegetation in cold regions hydrology.

84 **2. Model description and extensions for this paper**

85 **2.1 EcH₂O-iso model**

86 Recent advances in hydrological modelling have included more explicit process-based conceptualisation of ecohydrological
87 interactions (Fatichi et al., 2016) and the integration of tracer-based data (Birkel and Soulsby, 2015). The EcH₂O model (Maneta
88 and Silverman, 2013) was developed as an ecohydrological model coupling land-surface energy balance models with a physically-
89 based hydrologic model. This explicitly includes the dynamics of vegetation growth and vertical and lateral ecohydrological
90 exchanges.

91 *2.1.1 EcH₂O energy balance*

92 The energy balance is computed for two-layers, the canopy, and surface. The solution of the energy balance is used to calculate
93 the available energy reappportionment for transpiration, interception evaporation, soil evaporation, snowmelt, ground heat storage,
94 and canopy and soil temperature. The canopy energy balance is iteratively solved at each time step until canopy temperature
95 converges to the estimated value that balances radiative (incoming and outgoing short and long wave radiation), and turbulent
96 energy fluxes (sensible and latent heat) (Maneta and Silverman, 2013; Kuppel et al., 2018 a and b). Long- and shortwave radiation
97 transmitted through the canopy to the soil and longwave radiation emitted by the canopy toward the ground drive the surface
98 energy balance. The surface energy balance components include radiative exchanges (incoming and outgoing short and long-wave
99 radiation), sensible, latent, and ground heat fluxes, as well as heat storage in the soil and in the snowpack. While the energy balance
00 apportions energy to each storage (i.e. soil and snowpack), when the snowpack is present, estimated surface temperatures refer to
01 the snowpack surface and the ground is assumed to be at the temperature of the snowpack, which means that conductive heat
02 transfer between soil and snowpack is 0 (no thermal gradient). Also, when the snowpack is present latent heat for surface
03 evaporation is set to 0.

04 *2.1.2 EcH₂O-iso tracer and water age module*

05 EcH₂O has previously been adapted to incorporate the tracking of hydrological tracers including stable isotopes (Kuppel et
06 al., 2018b) and chloride (Douinot et al., submitted), and adapted to compute estimations of water age in water storage and fluxes.
07 Isotopic fractionation is simulated in soil water using the Craig-Gordon model (Craig and Gordon, 1965), and tracer mixing is
08 simulated using an implicit first-order finite difference scheme. Full details of the implementation of the isotopic module are in
09 Kuppel et al., (2018a). These adaptations do not consider fractionation of snowmelt or open water evaporation. Water ages are
10 estimated assuming complete mixing in each water storage compartment. Similar to other snowmelt tracer models (eg. Ala-aho et
11 al., 2017a), the snowmelt ages are defined as the time the snow enters the catchment, rather than the time of melt. This results in
12 older water estimations during the freshet period and a more complete estimate of the time that water has resided in the catchment.

13 **2.2 Soil water freeze-thaw adaptation**

14 Hydrology in cold regions can be greatly affected by the freeze-thaw cycles of soil water during the winter, resulting in
15 reduced liquid water storage capacity during the spring melt and a restricted capability for infiltration due to the expansion of ice
16 in pore spaces (Jansson, 1998). The depth of the soil frost can have a large influence on the timing of snowmelt runoff and provide



17 an estimation of the liquid water available within a soil layer (Carey and Woo, 2005). The Stefan equation is a simple energy
 18 balance approach to estimate the progression of soil water freezing (Jumikis, 1977):

$$\Delta z_f = \left[\frac{2k_f(T_s - T_f)}{\lambda\theta} \right]^{1/2} \quad (1)$$

19 where Δz_f is the change in depth of the frost and is a function of the thermal conductivity of the frozen soil layers between the frost
 20 depth and the soil surface (k_f), the soil surface temperature (T_s), the temperature of freezing (T_f), the latent heat of freezing (λ), and
 21 the liquid soil moisture (θ). As with previous approaches (Jumikis, 1977; Carey and Woo, 2005), the progression of the soil frost
 22 is estimated by discretizing the total soil depth into smaller layers. Within EcH₂O-iso, the sub-surface soil regime is discretized
 23 into three soil layers, layer 1 (near the surface), layer 2, and layer 3 (groundwater to bedrock), to resolve the water balance and
 24 estimate soil moisture. Here, the depths of layer 1, 2, and 3 were used as the layers since they intrinsically incorporate the soil
 25 moisture estimations without additional parameterisation. The thermal conductivity of frost affected layers is dependent on the
 26 moisture content of the soil:

$$k_f(i) = (k_{sat} - k_{dry}) \cdot \left(\frac{\theta(i)}{\phi(i)} \right) + k_{dry} \quad (2)$$

27 where $k_f(i)$ is the thermal conductivity of frozen soil in layer i , k_{sat} is the thermal conductivity of saturated soil, k_{dry} is the thermal
 28 conductivity of dry soil, $\theta(i)$ is the soil moisture in layer i , and $\phi(i)$ is the soil porosity in layer i . The saturated thermal conductivity
 29 was estimated from the proportions of soil comprised of ice, liquid water, air, organic material, and mineral soil (Carey and Woo,
 30 2005):

$$k_{sat} = \prod_{n=1}^5 k(j)^{f(j)} \quad (3)$$

31 where j is the thermal conductivity of each volume proportion, f is the fraction of total soil volume, and k is the thermal
 32 conductivity of volume j . Without proportions of soil organic and mineral material, the bulk soil thermal conductivity (k_{dry}) is
 33 considered the weighted average of organic and mineral thermal conductivity (only 4 total volumes in Eqn 3). Implementation of
 34 Eqns 1-3 are ideal for EcH₂O as the model estimates the parameters (T_s , and θ) or includes parameterisation of physical
 35 properties (λ , k_{dry} , ϕ , k_{water} , k_{air}), and only requires the addition of the thermal conductivity of ice (2.1W/m°C, Waite et al., 2006).
 36 Within EcH₂O, the estimation of surface temperature is assumed to be isothermal with the snowpack and conduction through the
 37 snowpack is not considered. However, the surface temperature used within the Stefan equation (Eqn 1) is the surface temperature
 38 below the snowpack. To address the conduction through the snowpack, the estimated surface temperature (T_{Est}) was damped
 39 with a single unitless parameter (D) such that $T_s = T_{Est}D$.

40 To account for the reduction of the infiltration rate due to ice, models have previously adjusted the soil hydraulic conductivity
 41 (e.g. Jansson, 1998). Here, the reduction in hydraulic conductivity is estimated using an exponential function:

$$K_{wf} = 10^{f \cdot c \cdot F} K_{sat} \quad (4)$$

42 where K_{wf} is the hydraulic conductivity of the soil influenced by ice, K_{sat} is the saturated hydraulic conductivity of ice-free soils, f
 43 is an ice-impedance parameter, and F is the fraction of frost depth to total soil depth. Equation (4) has two key assumptions: no ice
 44 lenses or frost heaving, and no soil volume expansion due to lower ice density (assumed 920kg/m³ at ice temperature 0-5°C).

45 2.3 Soil frost volume, depth, and water age

46 As soil frost progresses through the layers, the proportion of liquid water is assumed to decrease at the same rate as the
 47 proportion of unfrozen soil. Similar to other approaches estimating the moisture content of frost-affected soils (Jansson, 1998), a
 48 minimum liquid soil moisture was retained in all frozen soils. This minimum was assumed to be the residual soil moisture (θ_r),
 49 the minimum moisture content required for evaporation and root-uptake. The change in soil moisture of each layer is estimated:



$$\Delta\theta = (\theta(i) - \theta_r) \cdot \frac{\Delta z_f}{d(i) - d_f(i)} \quad (5)$$

50 where $\Delta\theta$ is the change in liquid water and ice content, $\theta(i)$ is the initial liquid content in layer i , θ_r is the residual moisture
 51 content, $d(i)$ is the total depth of layer i , and $d_f(i)$ is the depth of frost in layer i . Step-wise estimation of freeze and thaw for each
 52 layer is provided in more detail in Appendix A. The water age of the ice is estimated in a similar way to the liquid water ages of
 53 the soil layers (Kuppel et al., 2018b):

$$V_{res}^{t+\Delta t} A_{res}^{t+\Delta t} - V_{res}^t A_{res}^t = q_{in} A^{t+\Delta t} - q_{out} A_{res}^{t+\Delta t} \quad (6)$$

54 where t is time, Δt is the time-step, V_{res} is the volume of ice in storage, q_{in} is the volume of water from the change in soil moisture
 55 during freeze-up (from Eqn 5), q_{out} is the volume of water from the change in soil moisture during thaw (from Eqn 5), and A is
 56 the water age (subscripts res and in are the water ages in storage and inflow, respectively). Similar to the isotope and vegetation
 57 modules in EcH₂O, the frost dynamics (i.e. frost depths and water ages) were implemented as an option within EcH₂O.

58 2.4 Isotope snowmelt fractionation

59 Isotopic fractionation of snowmelt can have a significant influence on the composition of streams (Ala-aho et al., 2018a).
 60 Previous successful applications of a simple approach equation to estimate the isotopic fractionation of snowmelt at multiple
 61 locations has shown that low-parameterised fractionation models can be used to spatially approximate snowmelt fractionation. One
 62 of the noted limitations of the simple snowmelt fractionation approach used in Ala-aho et al., (2018), is the dependence of the
 63 snowmelt fractionation on the past snowmelt volumes rather than current snowmelt rate. The approach was modified to include
 64 the snowmelt rate with one additional parameter using an exponential function:

$$\delta^2 H_{melt} = \delta^2 H_{pack} - \left(S \cdot \exp \left(-S \cdot \left(1 - \frac{SWE - M}{SWE_{max}} \right) \right) \right) \cdot C \quad (7)$$

65 where $\delta^2 H_{melt}$ is the isotopic composition of the snowmelt, $\delta^2 H_{pack}$ is the composition of the snowpack at the beginning of the time-
 66 step, SWE is the snow water equivalent at the current time, SWE_{max} is the maximum snow water equivalent before melt, M is the
 67 total volume of snowmelt in the current time-step, S is a slope parameter describing the shape of the exponential change of the
 68 snowmelt fractionation, and C is an amplification factor. Higher values of S (10-20) result in larger early melt fractionation and
 69 limited late melt fractionation, while low values of S result in a lower, but more consistent fractionation throughout the melt period.
 70 The isotopic composition of the snowpack is updated at the end of each time-step.

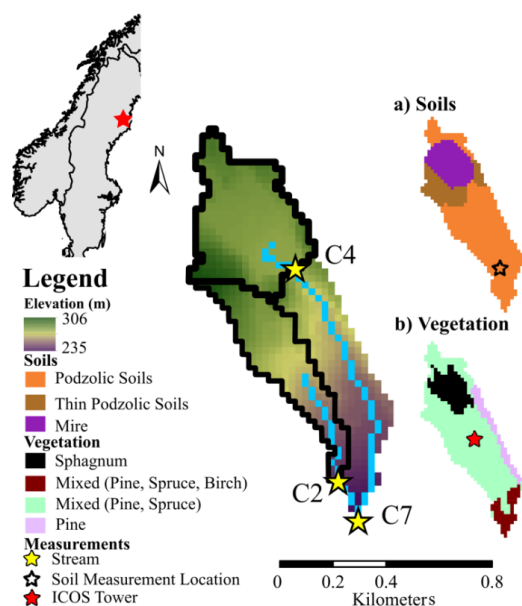
71 3. Data and study site

72 3.1 Study site

73 Svartberget (C7, 0.49 km²) is a small subcatchment situated in the headwaters of the Krycklan catchment (64°, 14'N, 19°46'E)
 74 in northern Sweden. Svartberget is a well-studied site with long-term data collection including: streamflow (1991-present), stream
 75 chemistry (2000-present), and hillslope transect measurements (soil moisture and water chemistry). Svartberget has two
 76 subcatchments, Västrabäcken (C2, 0.12 km²) and Mire (C4, 0.18 km²) (Fig. 1). The topographic relief of C7 is 71 m (235 – 306 m
 77 a.s.l.), with 57 m of relief in C2 (247 – 304 m a.s.l.) and only 26 m of relief in C4 (280 – 306 m a.s.l.) (Fig 1). The climate is
 78 subarctic (in the Köppen classification index), with annual precipitation of 614 mm, evapotranspiration (ET) of 303 mm, mean
 79 relative humidity of 82 %, and a 30 year mean annual temperature of 1.8 °C (Laudon et al., 2013). The relatively low topography
 80 results in no observable influence of elevation on precipitation (Karlsen et al., 2016b). The catchment experiences continuous
 81 snowpack development throughout the winter, accounting for approximately a third of the annual precipitation and lasting on
 82 average 167 days (Laudon and Löfvenius, 2016). The large quantity of snowfall results in a dominant snowmelt-driven freshet
 83 period (Karlsen et al., 2016a). Till (10 – 15 m thick) covers the majority of the downstream catchment area (C7, 92% downstream



84 of C4) with intermittent shallow soils in the headwaters of C2 (Fig. 1a). The catchment is predominantly forest covered (82% total,
85 98% downstream of C4), with Scots Pine (*Pinus sylvestris*), Norway Spruce (*Picea abies*), and Birch (*Betula spp.*). The Mire (Fig
86 1b) is dominated by *Sphagnum* mosses.



87
88 **Figure 1: Location of the Svartberget within Sweden and its elevation profile with the channels and stream measurement locations**
89 **(yellow). Inset figures show (a) catchment soils, and (b) catchment vegetation.**

90 3.2 Model data

91 3.2.1 Stream discharge and isotope datasets

92 The discharge at the three streamflow locations has been measured with hourly stream stage measurements using pressure
93 transducers. V-notch weirs improve measurement accuracy, aided by monthly salt dilution gauging to validate results. Average
94 discharge in the catchment varies from $9 \times 10^{-4} \text{ m}^3/\text{s}$ (C2) to $4 \times 10^{-3} \text{ m}^3/\text{s}$ at the outlet (C7), with maximum discharge events up to
95 $0.1 \text{ m}^3/\text{s}$ (C7) during spring freshets ($0.02 \text{ m}^3/\text{s}$ and $0.03 \text{ m}^3/\text{s}$ at C2 and C4, respectively). Stable isotopes $\delta^2\text{H}$ and $\delta^{18}\text{O}$
96 determinations were carried out for samples collected every two weeks at each site. Long-term average $\delta^2\text{H}$ is similar between
97 streams (-95.5 , -94.5 and -95.6 ‰ for C7, C2, and C4 respectively), with the highest isotopic variability at site C4 (standard
98 deviation (SD) of 7.9 ‰) and lowest at C2 (SD of 4.5 ‰) with C7 intermediate.

99 3.2.2 Meteorological datasets

00 Precipitation (rain and snowfall), temperature, wind speed, and relative humidity were measured daily at the Svartberg
01 meteorological station, 150 m southwest of the catchment. Radiation data, incoming longwave and shortwave radiation, were
02 obtained at 3-hourly time-steps and $0.75 \times 0.75 \text{ km}$ grid resolution from ERA-Interim climate reanalysis (Dee et al., 2011). During
03 the study, a 150 m observation tower (Integrated Carbon observation system, ICOS Tower) was installed within the catchment.
04 Data from the ICOS tower were available from 2014 to 2015. The ICOS tower measures energy fluxes, latent and sensible heat,
05 and net radiation, among other atmospheric parameters. The isotopic composition of precipitation was determined on daily bulk
06 samples following each major rain and snow event. The average precipitation $\delta^2\text{H}$ (weighted mean -95.1 ‰) is similar to the stream
07 isotopic composition, though the isotopic variability is between 4.4 – 7.8 times larger.



08 **Table 1: Datasets used for forcing, calibration and validation within the Svartberg catchment**

Input Meteorological Forcing Data			
Air Temperature (minimum, maximum, and mean) (°C)	Svartberg	Daily	2005-2016
Precipitation (m/s)	Svartberg	Daily	2005-2016
Wind speed	Svartberg	Daily	2005-2016
Relative Humidity	Svartberg	Daily	2005-2016
Longwave Radiation	ERA-interm	Daily	2005-2016
Shortwave Radiation	ERA-interm	Daily	2005-2016
δ ² H Precipitation	Svartberg	Event-based	2005-2016
Calibration and Validation Datasets			
	Location	Resolution	Time-Period
Discharge	C7	Hourly	2005 – 2016
	C2	Hourly	2005 – 2016
	C4	Hourly	2005 – 2016
Stream isotopes	C7	Biweekly	2005 – 2016
	C2	Biweekly	2005 – 2016
	C4	Biweekly	2005 – 2016
Soil Moisture	S12	Hourly at depth of 5, 10, 20, 30, 40, 60 cm	2013 – 2016
	S22	Hourly at depth of 6, 12, 20, 50, 60, 90 cm	2013 – 2016
Validation Only Datasets			
	Location	Resolution	Time-Period
Soil Isotopes (Lysimeter)	S12	9 samples: 10, 20, 30, 40, 60, and 70 cm	2012
	S22	9 samples: 10, 20, 35, 50, 75, and 90 cm	2012
Soil Isotopes (Bulk Water)	S12		2015 – 2016
	S22	7 samples: 10, 20, 30, 40, 60, and 70 cm	2015 – 2016
Soil Temperature		30 min @ 4 locations at depths 5, 10, 15, 30, and 50 cm	2014 – 2015
Net Radiation	ICOS	30 min	
Latent Heat	Tower	30 min	
Sensible Heat		30 in	

09

10 **3.2.3 Soil moisture and isotope datasets**

11 Soil moisture sensors were installed in 1997 and replaced at the beginning for 2013. The soil moisture sensors were installed
 12 at the hillslope transect location at 4, 12, 22, and 28 m locations from the C2 stream. The depths of the soil moisture measurements
 13 slightly differ between sites (Table 1); however, the depths encompass shallow and deep soil waters. Soil sensors have also been
 14 installed in the area surrounding the ICOS tower, measuring soil temperature at 4 locations and 6 depths (10, 20, 30, 40, 60, and
 15 70 cm) (Table 1) which can provide a proxy for the depth of the frost. Soil isotopes (δ²H and δ¹⁸O) were measured at multiple
 16 depths (2.5 cm increments) measured via lysimeters (2012) and bulk water samples (2015 – 2016).

17 **3.3 Model set-up and calibration**

18 The C7 catchment was defined with a grid resolution of 25 × 25 m² to balance adequate differentiation of multiple locations
 19 on the soil water transect while maintaining computational efficiency. The 25 m grid includes adjacent soil pixels for S12 and S22,
 20 with sites S04 and S28 within the same grids as S12 and S22, respectively. All simulations were conducted on a daily time-step
 21 between January 2005 and September 2016. The period from January 2005 to December 2009 was used as a spin-up period with
 22 measured hydrologic data, to stabilize δ²H, δ¹⁸O composition, and water ages in each of the model storage units. Initial analysis of
 23 the measured discharge from 2000-2016 revealed the highest and lowest annual discharge years were between 2010 and 2014.
 24 Consequently, calibration was carried out for the period between January 2010 and December 2014. The validation set used was
 25 the remaining period from January 2015 – September 2016. Within the biomass module, the vegetation dynamics for leaf growth



26 and carbon allocation were held at steady state to minimize the parameterisation and focus on the soil freeze-thaw cycles. As
27 temperature effects and water stress are less sensitive for conifer trees, a relatively constant leaf area index and needle growth/decay
28 rate were maintained (Liu et al., 2018). Evaporative soil water fractionation was activated using similar parameterisation to Kuppel
29 et al. (2018b), as this has previously been identified as an influential summer process in the catchment (Ala-aho et al., 2017a). Soil
30 relative humidity was estimated using Lee and Pielke's (1992) approach, and values of kinematic diffusion were estimated as
31 presented by Vogt (1976) (0.9877 and 0.9859 for H^2/H^1 and O^{18}/O^{16} ratios, respectively). Parameterisation of the model was
32 conducted for each soil type (3 soil types, Fig 1a) and vegetation type (4 types, Fig 1b).

33 A sensitivity analysis established the most sensitive parameters to be used in calibration using the Morris sensitivity analysis
34 (Soheir et al., 2014). Parameters were assessed using 10 trajectories using a radial step for evaluating the parameter space. The
35 parameter sensitivity was evaluated using the mean absolute error. Results of this are shown in Appendix B. Sensitive parameters
36 were calibrated using Latin Hypercube sampling (McKay et al., 1979) with 150,000 parameter sets and a Monte Carlo simulation
37 approach to optimize the testing of the model parameter space.

38 **3.4 Model evaluation**

39 The model output was constrained using measurements of stream discharge (3 sites, Fig. 1), stream δ^2H (3 sites, Fig. 1), and
40 soil moisture (2 sites, Fig. 1a). The 8 measurement datasets were combined into a multi-criteria calibration objective function using
41 the mean absolute error (MAE) with the cumulative distribution functions (CDFs) of the model goodness-of-fit (GOF) (Ala-aho
42 et al., 2017a; Kuppel et al., 2018 a and b). The MAE moderated over-calibration of peak flow events, typical for functions like the
43 root mean square error, and Nash-Sutcliffe efficiency, as well as being consistent with previous studies in the region (Ala-aho et
44 al., 2017a). To focus on the dynamics of soil moisture, given the coarse model grid, measured and simulated values were
45 normalized by their respective mean values prior to analysis. From the CDF method, the 30 "best" simulations were selected for
46 evaluation and are presented using 95% spread of predictive uncertainty (Kuppel et al., 2018b). The parameters achieved through
47 calibration are shown in Appendix C. Model results were verified against the remaining years of discharge, soil moisture, and
48 stream flow δ^2H , as well as independent time series of soil isotopes (bulk and lysimeter), net radiation, sensible heat, latent heat,
49 and frost depth (estimated from depth-dependent soil temperatures).

50 The evaluation of changes to water ages due to soil frost was conducted by comparing the ages within the catchment for
51 simulations of the 30 "best" parameter sets with and without frost. These were conducted without frost by turning frost dynamics
52 off within the model. Freeze-thaw effects on evaporation and transpiration ages were evaluated as the difference between frost and
53 non-frost simulations. Positive values indicate older water with the frost while negative values indicate older water with frost-free
54 simulations. The age differences were only considered on days when both frost and non-frost simulations simulate a flux greater
55 than 0 mm/day.

56 **4. Results**

57 **4.1 Simulation results**

58 Calibration captured dynamics of both high and low flow discharge periods through both the calibration period (2010 – 2014)
59 and validation period (2015 – 2016), with a maximum mean stream flow MAE of $2 \times 10^{-3} \text{ m}^3/\text{s}$ for C7, and a maximum mean stream
60 δ^2H MAE of 5.8 ‰ at C4 (Table 2). Due to extreme high and low flow periods in the calibration period, it was unsurprising that
61 the resulting MAE was higher than in the validation. The MAE of the soil moisture calibration was also reasonable, with average
62 MAE of 0.05 and 0.09 for sites S12 and S22, respectively. With the normalization of the soil moisture, the low MAE indicates that
63 the dynamics in the model correspond well to those measured. The optimization of the GOF for 3 measures (discharge, stream

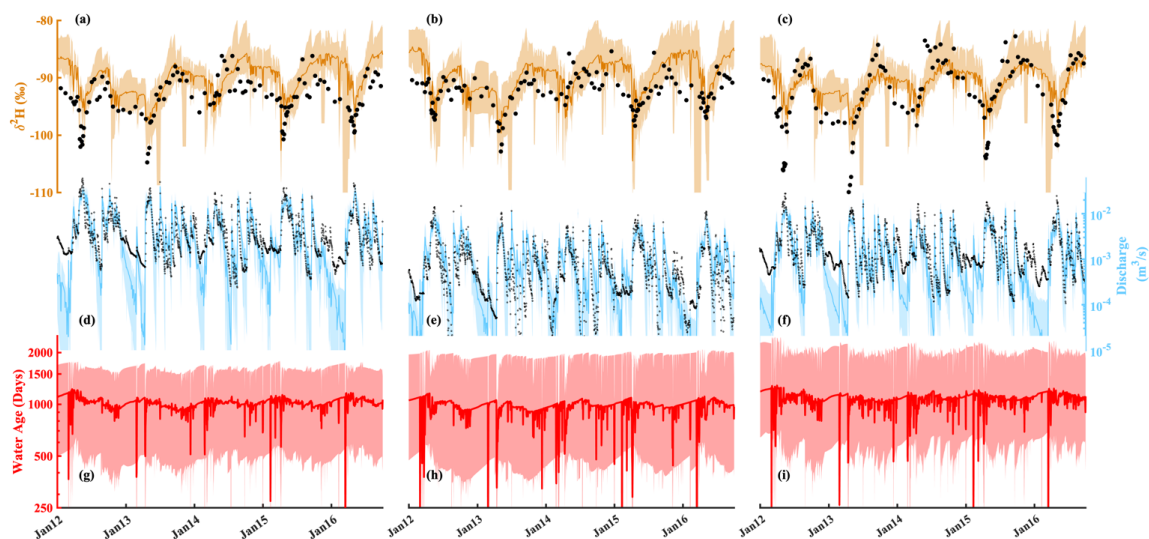


64 $\delta^2\text{H}$, and soil moisture) at 8 locations resulted in a compromise for all streams. Simulations yielded better (lower) MAE for
 65 discharge and isotopes of individual streams.

66 **Table 2: Calibration and validation efficiency criteria, shown as mean efficiency for all multi-calibration criteria**

		Calibration (2010 – 2014)	Validation (2015 – 2016)
	Site	MAE	MAE
Discharge	C7	$2 \times 10^{-3} \text{ m}^3/\text{s}$	$6 \times 10^{-4} \text{ m}^3/\text{s}$
	C2	$1 \times 10^{-3} \text{ m}^3/\text{s}$	$1 \times 10^{-4} \text{ m}^3/\text{s}$
	C4	$1 \times 10^{-3} \text{ m}^3/\text{s}$	$3 \times 10^{-4} \text{ m}^3/\text{s}$
$\delta^2\text{H}$	C7	4.8 ‰	4.0 ‰
	C2	4.6 ‰	3.8 ‰
	C4	5.8 ‰	3.9 ‰
Soil Moisture	S12	0.05	0.09
	S22	0.09	0.09
Latent Heat	ICOS Tower	N/A	13.1 W/m ²
Sensible Heat	ICOS Tower	N/A	29.5 W/m ²
Net Radiation	ICOS Tower	N/A	31.0 W/m ²
Soil Frost Depth	ICOS Tower	N/A	0.03 m

67 Temporal variability of $\delta^2\text{H}$ in each of the streams was captured quite well throughout the calibration and validation periods
 68 (Fig 2 a – c). The largest offsets in modelled isotopic composition occurred during the winter low flow conditions. The simulated
 69 stream isotopes tended to retain a slight “memory” effect from the more enriched late summer. This was likely due to the
 70 underestimation of discharge during winter (Fig 2 d – f) which slowed the flushing of the more enriched water. Overall though,
 71 discharge was adequately simulated for each site, notably during the spring melt and summer months. While flows were
 72 underestimated during the winter, the difference between simulations and measurements were typically $< 1 \times 10^{-3} \text{ m}^3/\text{s}$. The weight-
 73 median water ages of each of the three streams were broadly similar, 2.8, 2.6, and 3.1 years for C7, C2, and C4, respectively (Fig
 74 2 g – i). These stream ages were generally older than previous estimates, with deeper soil layers and complete mixing in each
 75 compartment tending to increase the average age. The depth of the soil layers in the peat and podzolic areas are the primary drivers
 76 for water age, with a ~1:1 relationship (Appendix D). Water age decreased during the annual freshet, driven by the younger
 77 snowmelt and frozen soil water ages (typically 150 – 200 days old). The rapid runoff during the freshet limited the long-term
 78 influence of the younger water ages on the stream water at each of the sites as older groundwater dominated low flows.

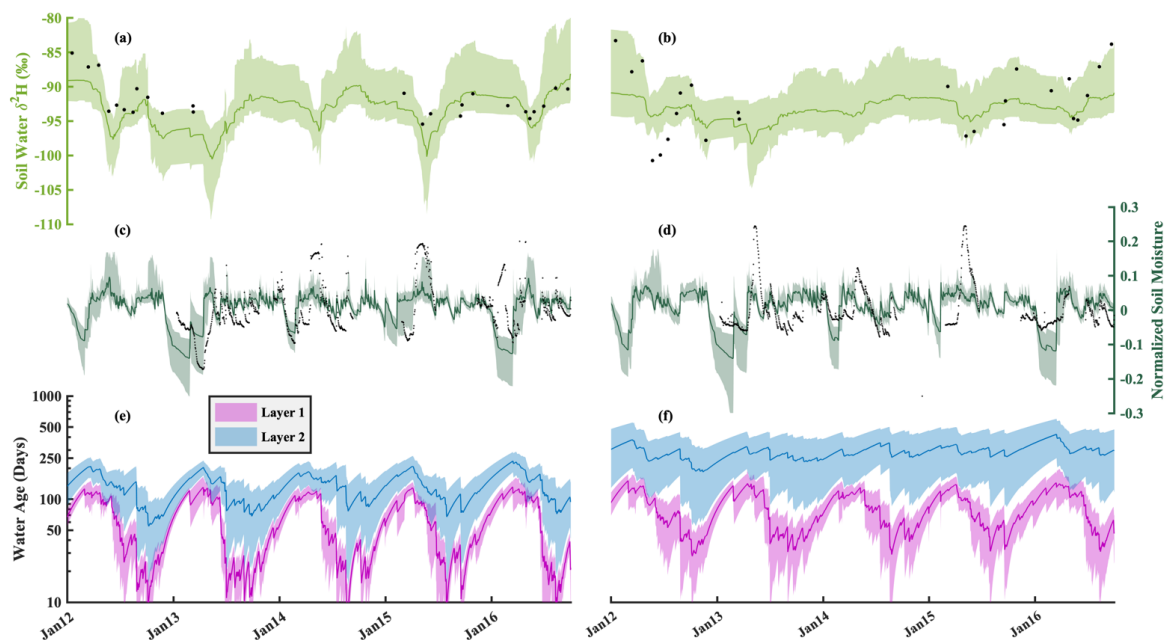


79

80 **Figure 2: Calibration 95% maximum and 5% minimum bounds, median simulation (solid line), and measured data (black circles) of**
81 **$\delta^2\text{H}$ for (a) C7, (b) C2, and (c) C4; discharge for (d) C7, (e), C2, and (f) C4; and stream water age for (g) C7, (h) C2, and (i) C4.**

82 **4.2 Soil moisture, isotope, and water ages**

83 Simulated soil water isotopes (note that the model did not use isotopes during calibration) mostly captured those measured in
84 both bulk water (2015 – 2016) and lysimeter water (2012) within the 90% simulation bounds at the S12 and S22 sites (Fig 3 a &
85 b). Isotope dynamics were best captured at site S12, with early season depletion due to snowmelt and enrichment of the previous
86 summer. While most variability was captured within the 90% bounds, the magnitude of the intra-annual contrasts at site S22 was
87 not fully reproduced. Similar to the soil isotopes, dynamics of simulated soil moisture (calibrated) were captured at both S12 and
88 S22, with better simulation performance at S12 (Fig 3 c & d). The model struggled to simultaneously reproduce the more dynamic
89 soil moisture at S12 with the relatively damped soil moisture post-melt at S22 in the adjacent cell under the same soil
90 parameterisation. Rather, the same parameterisation resulted in balancing the conditions observed at S12 and S22. The large
91 declines in measured soil moisture during the winter months were captured with the soil frost module (Fig 3 c & d). The modelled
92 decline in the soil moisture resulted from the transition of soil water from liquid to ice. Water ages in layers 1 and 2 at each site
93 showed noticeable intra-annual variability, and gradually declined during the growing season (May – September) and increased
94 during the winter due to negligible water inflow (Fig 3 e & f). The variability of the soil water ages in layers 1 and 2 was similar,
95 though the ages in layer 2 were significantly older. While S12 is closer to the stream, water ages in S22 were generally older in
96 both layers 1 and 2.

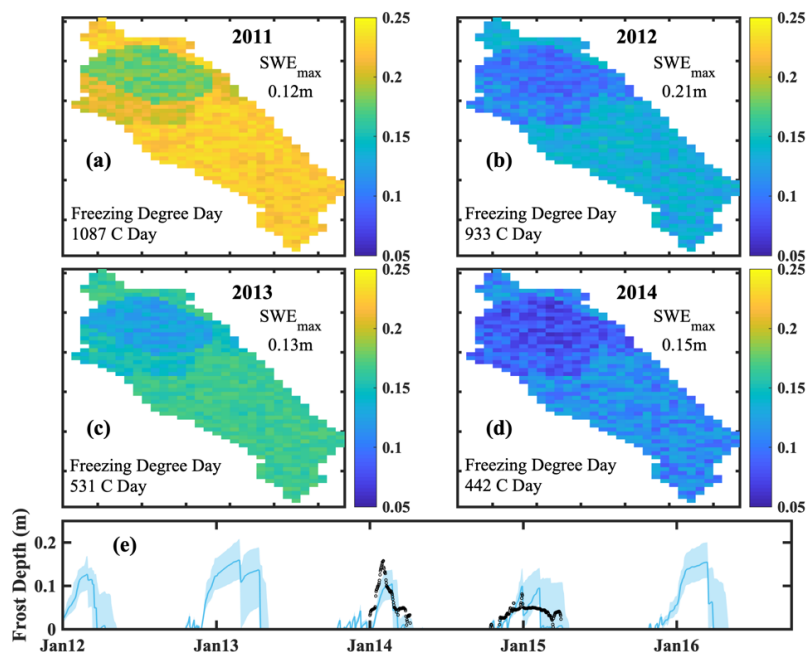


97

98 **Figure 3: Simulation 90% bounds and mean simulation (solid line) for the average of layer 1 and 2 $\delta^2\text{H}$ for (a) site S12, and (b) site S22;**
99 **the average of layer 1 and 2 normalized soil moisture for (a) site S12 and (b) site S22; and water ages of soil layers 1 and 2 for (e) site**
00 **S12, and (f) site S22.**

01 **4.3 Soil freeze-thaw simulations**

02 Simulations of frost depth revealed large inter-annual variability throughout the catchment (Fig 4 a-d), depending on winter
03 temperatures, snowpack depth, and the soil moisture conditions. Wetter conditions in the mire generally show shallower frost
04 depths than the podzolic soils elsewhere in the catchment. Similar soil conditions for the podzolic and thin podzolic soils (Fig 1a)
05 resulted in negligible differences for estimated frost depth. Overall, estimated frost depth was generally limited by the total number
06 of freezing days. Colder winters (larger numbers of freezing degree days) resulted in deeper frost depths for an equivalent snowpack
07 depth (e.g. Fig 4a vs Fig 4c). Conversely, a deeper snowpack (higher maximum SWE) resulted in a shallower simulated frost depth
08 for years with similar temperatures (e.g. Fig 4a vs c) as the deeper snowpack was a larger storage for incoming radiation. Using
09 0°C in the soil temperature probes at the ICOS tower as a proxy for the depth of the soil frost, a direct comparison of simulated
10 frost depth and the measured catchment frost depth was completed without calibration. Simulated frost depth showed good
11 agreement with observed 0°C soil temperature depth, imitating the rapid increase in frost depth in 2014 and a more gradual increase
12 in 2015 (Fig 4e). Late winter soil frost depth was estimated to be shallower and varied more rapidly than the observed 0°C soil
13 temperature depth (Fig 4e). The median estimated soil depth against the measured 0°C soil temperature depth showed that estimate
14 soil thaw was too rapid, and thaw completed too early.



15

16 **Figure 4:** Mean simulated soil frost depth during the peak soil frost depth in winter (a) 2010-2011, (b) 2011-2012, (c) 2012-2013, and (d)
 17 2013-2014. 90% uncertainty bounds of the simulated frost depth at the ICOS Tower with the depth of the 0°C soil temperature measured
 18 at the ICOS Tower (black circles)

19 **4.4 Evaporation and transpiration**

20 While the evaporation, transpiration, and energy balance datasets were not included in the calibration, modelled energy balance
 21 components (sensible heat, latent heat, and net radiation) showed reasonable agreement to observed values in 2014-2016 at the
 22 ICOS Tower. There was an under-estimation of net radiation and sensible heat throughout the growing season (Fig 5 b & c), and
 23 an underestimation of latent heat late in the year (Fig 5a). While the MAE of the latent heat was relatively small (13.1 W/m²)
 24 considering that they were not used for calibration, net radiation and sensible heat had a notable maximum bias (~30 W/m²) during
 25 summer. Simulations of total daily evaporation (soil and interception) and transpiration had a similar pattern, with transpiration
 26 accounting, on average, for 54% of total evapotranspiration. Throughout the year, the simulated proportion of transpiration to total
 27 evapotranspiration ranged from 31 – 72% except for the spring periods (Fig 5d). The late onset of evaporation resulted from the
 28 assumption that soil evaporation was negligible while the snowpack remains, which potentially lead to an under-estimation of
 29 evaporation during the melt.

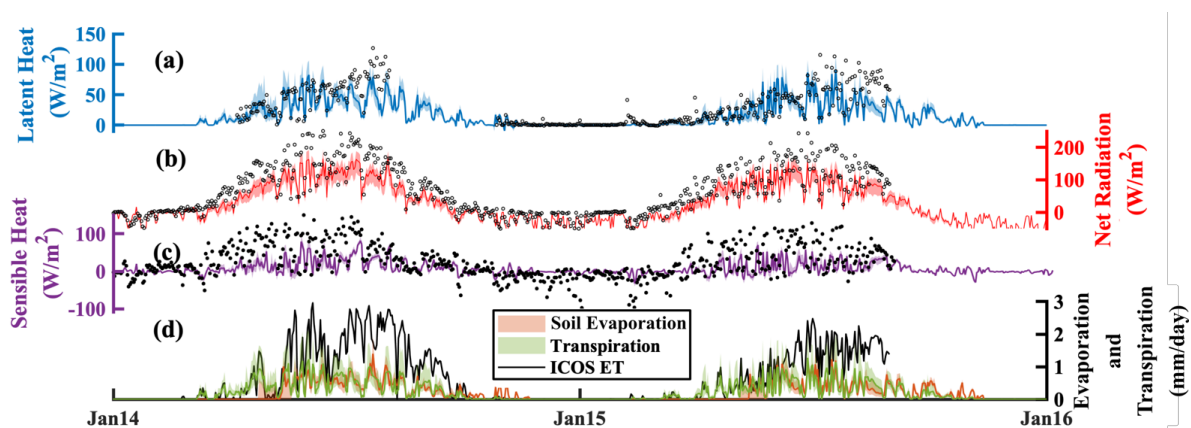
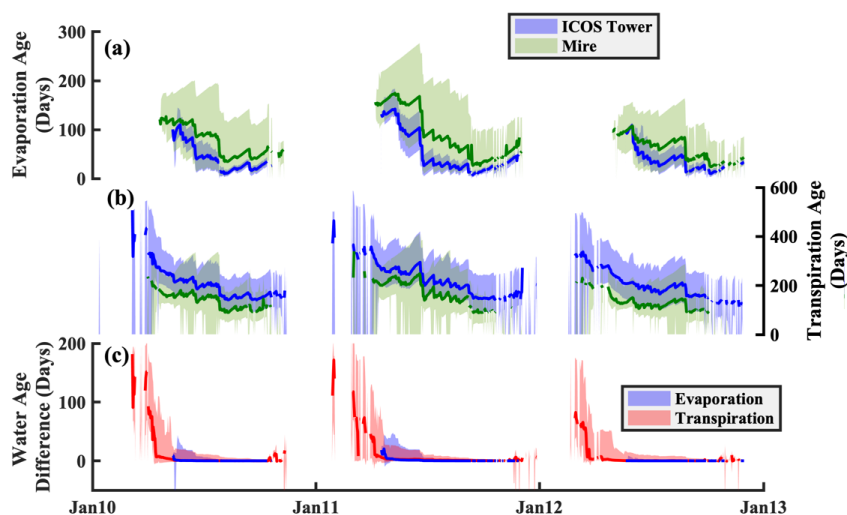


Figure 5: Energy balance component of (a) estimated latent heat (90% and mean values), (b) estimated net radiation (90% and median values), (c) estimated sensible heat (90% and median values) and (d) estimated soil evaporation and transpiration (90% and mean values), at the ICOS Tower site with the estimated total evapotranspiration from energy fluxes at the ICOS Tower (black circles where data are available).

Ages of soil evaporation and transpiration decreased throughout the year (Fig 6 a and b), tracing the decline in soil water ages estimated with the addition of precipitation (age of 0 days). Older water present in evaporation and transpiration water at the start of the year was a mixture of the snowmelt water age and frozen water ages (from the previous summer). Spatial differences in evaporation and transpiration ages were evident throughout the catchment; shown by the difference between the forested ICOS tower site (blue, Fig 6 a & b), and the average for shrubs in the mire (green, Fig 6 a & b). The annual flux-weighted median water age of transpiration was 200 ± 42 and 141 ± 40 days for the ICOS tower and mire, respectively, while evaporation ages were 48 ± 11 and 85 ± 36 days for the ICOS tower and mire, respectively. Shallower roots of the shrubs resulted in younger transpiration ages than at the ICOS tower and subsequently resulted in older evaporation ages in the mire due to reduced availability of young water.

Differences between the evaporation and transpiration ages were determined by comparing water ages with the soil frost module activated, against those with the frost module deactivated. Generally, including frost in the simulations resulted in older water (water age difference > 0 Fig 6c) for both evaporation and transpiration. Differences in evaporation age were not as pronounced as transpiration ages due to the slight bias of the evaporation timing (always following the snowmelt). Due to the estimated completion of soil thaw prior to the snowmelt period, the difference between the water ages of evaporation with the influence of frozen ground was modest. Rapid flushing of the soil water due to large snowmelt inputs and spring precipitation resulted in a rapid decline in the differences of transpiration water ages. Within the first month of transpiration, the difference for the frost and non-frost simulations were more notable and approached 200 days when frost limited water movement. However, the relatively lower transpiration rates, which occurred during the spring within these simulations, resulted in a moderate effect on the overall annual transpiration water ages. The effects of soil frost on stream water ages showed little effect, with negligible differences given the relatively old water bias in the stream that only shows some flashes of younger water influence (Fig 2 g – i). While the soil frost increased the stream water ages throughout the year, the effect is well within the relatively large uncertainty bounds of the stream water ages.



58

59

60

61

Figure 6: 90% bounds and median values of the (a) estimated soil evaporation water ages at the ICOS Tower (blue) and in the Mire (green), (b) estimated transpiration water age at the ICOS Tower (blue) and in the Mire (green), and (c) mean difference of evaporation and transpiration water ages when soil frost is not considered.

62

5. Discussion

63

5.1 Modelling soil freeze-thaw processes in tracer-aided models

64

65

66

67

68

69

70

71

72

73

74

75

76

77

78

79

80

81

82

83

84

Hydrologic models are powerful tools for exploring the internal functioning of catchments, particularly when intensive and long-term monitoring programs are in place to help calibration and testing (Maxwell et al., 2019). Here, the development of a spatially distributed, process-based tracer-aided model for northern climates produced encouraging results reproducing soil frost dynamics despite the model not being directly calibrated to match frost depths observations. The use of streamflows, stream isotope ratios and soil moisture dynamics in calibration proved to be adequate for estimating the dynamics of soil frost depth and timing of the frost onset (Fig 4) and revealed spatial differences in frost depth due to contrasting soil types and moisture conditions. However, there are limitations with the current approach that results in some uncertainty of the effect of soil freeze-thaw on catchment hydrology. To improve the computational efficiency of the model, the temperature of the snowpack was assumed to be isothermal (Maneta and Silverman, 2013), and modified here to include only a single temperature damping parameter. However, snowpacks may have a variable thermal gradient (e.g. Filippa et al., 2014), and is dependent on snow density (e.g. Riche and Schneebeli, 2013), snow surface albedo, wind speed, and liquid water component, among others (USACE, 1956; Meløysund et al., 2007; Sturm et al., 2010). While these additional components may contribute to an improvement in the estimation of soil frost, it likely would not have a significant improvement compared to the simple temperature damping used here with additional calibration to constrain snow water equivalent for more dynamic energy exchange (e.g. Lindström et al, 2002). The simplistic consideration of negligible soil sensible heat storage effects on the soil freeze/thaw processes, consistent with other process-based cold region models (e.g. CHRMs, Xie and Gough, 2013), may result in dampened rates of freezing and rapid melting during the spring (Kurylyk and Hayashi, 2016). More delayed melting of the soil frost may have implications for snowmelt runoff, increasing the dynamics of the streamflow isotopic compositions towards more depleted isotopic compositions (Fig 2 a-c). Finally, the simplification of a single soil frost front may have some implications for the snowmelt infiltration to the soil. The single front does not allow for near-surface soil thaw to occur prior to deeper soils and thereby has implications for shallow root-water uptake and evaporation.



85 Energy fluxes in northern catchments can be highly sensitive to the timing of snowmelt, yielding differences in the surface
86 and canopy net radiation due to changing albedo and to turbulent fluxes due to alterations in surface temperature. Here, the under-
87 estimated sensible heat flux during the spring and the growing season could be the result of either the aerodynamic resistance (r_a)
88 to transpiration or an underestimated thermal gradient between the soil and the measured air temperature. Higher estimations in
89 early season surface temperatures could also result in the shallower, and earlier, simulated soil frost melt relative to the measured
90 0°C soil temperature depth. While improved timing of the soil-thaw period would likely improve this, direct calibration of the
91 sensible heat fluxes using the vegetation and soil albedo are likely more effective routes to improved simulations.

92 **5.2 Effect of soil freeze-thaw on water ages and implications for northern catchments**

93 The adaptation here of a process-based, spatially distributed model to incorporate some more fundamental aspects of the
94 hydrology of cold regions provides both the opportunity to improve the representation of key hydrologic functions of cold
95 catchments, and assess the effect that these additional processes have on transit times and ages of ecohydrological fluxes. While
96 some work has been conducted on assessing the transit or residence times of ecohydrologic fluxes or their partitioning in northern
97 (e.g. Sprenger et al., 2018a); however, few studies have included the influence of frozen conditions on the water movement, which
98 may be significant for the effective transit times during the spring freshet period (Tetzlaff et al., 2018) and flow path modelling in
99 regions (Laudon et al., 2007; Sterte et al., 2018). Traditionally, water ages in stream water at catchment outlets have been the
00 primary metrics for assessing the transport of tracers. Here, the relatively old age of stream water, and the under-estimation of soil-
01 thaw result in only slightly older water ages when soil frost conditions are considered, potentially due to the smaller proportion of
02 wetland areas (Sterte et al., 2018). The deeper frost depth in the forested regions likely did not reduce the spring infiltration due to
03 the low moisture content in the soil relative to the more saturated wetlands (Laudon et al., 2007). Additionally, the relatively wide
04 uncertainty bounds of stream water age estimates present difficulties in assessing the relatively moderate effects of soil frost on
05 the stream water age (Fig 2). The large dependence of the flows and stream water ages at C7 on the outlet of the large mire at C4
06 indicates that the water age progressing through the mire will be a strong determinant of long-term change. The flux-weighted
07 median water age estimations for the streams here were estimated to be substantially older than other tracer-aided hydrologic
08 models for the catchment (Ala aho et al., 2017a), though were on the upper end of other stream and hillslope transit times from
09 transit time methods (Peralta-Tapia et al., 2016; Ameli et al., 2017). The reasons for this are largely three-fold. Firstly, the model
10 was calibrated with soil depths comparable to those observed in the catchment. The calibrated model used soil depths ranging from
11 1.5 – 6 m, where the shallower soil depths yield stream water ages are comparable to previous studies. Secondly, the complete
12 mixing assumption within the model does not allow for rapid preferential movement of young water that has been observed in
13 numerous other recent studies (e.g. Botter et al., 2010; Harman 2015). Incomplete mixing within the model framework would
14 allow for deeper soil profiles to yield younger water fluxes, as estimated from isotopes alone, albeit at the expense of additional
15 parameterisation. Lastly, the previous transit time estimations (Peralta-Tapia et al., 2016; Ameli et al., 2017) do not account for
16 older water ages of the snowpack, or the immobility and aging of frozen soil water, which would increase the estimated water ages.

17 Unlike stream or soil water ages, low uncertainty of transpiration and soil evaporation ages helps bring new understanding to
18 how soil frost affects the source contributions of these ecohydrological fluxes which were the focus of the study. Ages of both
19 transpiration and soil evaporation are consistent with soil profile modelling conducted in the region using the SWIS model
20 (Sprenger et al., 2018b). However, the dynamics of the age variation are notably different due to the differences in the input water,
21 where the snowmelt input to the SWIS model assumes a water age of 0 days and does not account for the “green” water fluxes
22 during the spring months. While the transpiration ages show notable differences when frost, and the corresponding discontinuity
23 of transit times, is included in the simulation, the evaporation water ages are not greatly affected. The differences are reduced for
24 both fluxes due to a few potential reasons. Firstly, the timing of the soil thaw has a significant influence on age estimation of soil



25 water available for both evaporation and root-uptake. While the general timing and magnitude of the soil frost depth development
26 seems appropriately captured by the model, even without calibration, soil thaw in late winter was simulated faster than observations
27 (Fig 4e). There are notable differences between the ages of soil water, soil frost, and the snowpack, where soil frost is representative
28 of the previous fall soil water, soil water is a younger water mix of the fall soil water and newer precipitation (e.g. from rain-on-
29 snow and early spring snowmelt), and snowpack is the amount weighed age of solid precipitation. Here, shallower soil frost and
30 early melting of soil frost in the spring results in step-wise mixing, firstly of soil frost (oldest water) and soil water (moderate age),
31 then of the soil water mixture and snowmelt (youngest water). Since evaporation, and its corresponding age, only begins following
32 the end of snowmelt, the greater degree of mixing of soil frost ages with the soil water and snowmelt reduce the influence of the
33 soil frost on the evaporation ages. Delaying the simulated timing of soil thaw would result in a larger influence of the soil water
34 ages on both the evaporation and root-uptake.

35 While the influence of soil frost on stream water ages was limited in this catchment, the results have potentially significant
36 implications for modelling other catchments with frozen soils. The effect on water ages will likely be the greatest in catchments
37 where winter precipitation is limited, allowing the soil frost depth to increase from the surface, delaying the soil thaw until after
38 the primary snowmelt. For evaporation and transpiration water ages, notable spatial differences highlight an essential consideration
39 for northern climates in the influence of vegetation-type on the source of water fluxes. In many northern areas, past glaciation
40 results in significant wetlands typically dominated with shrub and herbaceous vegetation. Reductions in soil frost will result in
41 greater water availability throughout the year, aiding in vegetation growth (Woo, 2013). With the dominance of shallow rooting
42 profiles in short vegetation and their dependence on younger water, it is likely that the shrub-covered regions of the boreal
43 catchments will increase in their water usage, and increase the age of soil water and catchment outflows. Finally, the timing of the
44 evaporation and root-uptake needs to be strongly considered, at both seasonal and diurnal time scales. Soil frost had a strong
45 influence on the timing of evaporation and transpiration, where the magnitude of both fluxes was greater in simulations without
46 soil frost and timing of the root-uptake and soil evaporation was delayed due to ice-restricted pore spaces. While such changes are
47 anticipated, many studies have focused on plot scale studies and with estimated long-term reductions of soil frost depth, larger
48 scale estimations of these differences are essential to understanding how catchment ecosystems will respond.

49 **6. Conclusion**

50 In northern environments, with a rapidly changing climate, quantitative evaluation of vegetation interactions with catchment
51 soil water is crucial for understanding and projecting catchment responses. The process-based evaluation here of a well-monitored,
52 long-term study catchment in the northern boreal forest region using a tracer-aided, surface-atmosphere energy-balance model has
53 provided significant insights into the importance of soil freeze-thaw processes. Tracers were used, not only as a calibration tool,
54 but as validation metrics, and highlighted the effectiveness multi-criteria calibration of a model at nested scales using discharge,
55 isotopes, and soil moisture to constrain additional, un-measured, features (e.g. soil frost depth). The progressively younger ages of
56 evaporation and transpiration throughout the growing season show the dependence of both “green water” fluxes on spring
57 snowmelt, which remains in soil water towards the end of the growing season. Adaptation of the EcH₂O-iso model provided an
58 opportunity to examine spatial patterns of frost depth throughout the catchment and its ecohydrological influence. Soil frost
59 responded to both lower winter temperatures (increasing frost depths) and greater snowpack depth (decreasing frost depth). While
60 there was little influence on the overall timing of water movement at the catchment scale as stream water ages, the greatest influence
61 was observed within the ecohydrological partitioning, notably with the transpiration ages. Soil frost delays the onset of vegetation
62 growth and soil evaporation, resulting in older soil water from the previous autumn to sustain early-season transpiration rather than
63 younger snowmelt. With the implications of reduced numbers of cold days (Guttorp and Xu, 2011), and the dependence of



64 vegetation growth on the summer temperatures (Schöne et al., 2004) in northern latitudes, this assessment of ecohydrological
65 partitioning is timely in understanding the effect of climatic change.

66

67 **Acknowledgements**

68 This work was funded by the European Research Council (project GA 335910 VeWa). Marco Maneta recognises funding for
69 model development and applications from the US National Science Foundation (project GSS 1461576). The work in the
70 Krycklan catchment is funded by Swedish Research Council (SITES), SKB, Formas and the KAW program Branch-Points.

71 **References**

- 72 Ala-aho, P., Tetzlaff, D., McNamara, J. P., Laudon, H., and Soulsby, C.: Using isotopes to constrain water flux and age estimates
73 in snow-influenced catchments using the STARR (Spatially distributed Tracer-Aided Rainfall–Runoff) model, *Hydrol. Earth*
74 *Syst. Sci.*, 21, 5089–5110, doi:10.5194/hess-21-5089-2017, 2018a.
- 75 Ala-aho, P., Tetzlaff, D., McNamara, J.P., Laudon, H., Kormos, P., and Soulsby, C.: Modeling the isotopic evolution of
76 snowpack and snowmelt: Testing a spatially distributed parsimonious approach, *Water Resources Research*, 53(7), 5813–
77 5830, doi: 10.1002/2017WR020650, 2018b.
- 78 Ameli, A.A., Beven, K., Erlandsson, M., Creed, I.F., McDonnell, J.J., and Bishop, K.: Primary weathering rates, water transit
79 times, and concentration-discharge relations: A theoretical analysis for the critical zone, *Water Resources Research*, 53, 942–
80 960, doi: 10.1002/2016WR019448, 2017.
- 81 Birkel, C., and Soulsby, C.: Advancing tracer-aided rainfall-runoff modelling: a review of progress, problems and unrealised
82 potential, *Hydrological Processes*, 29(25), 5227–5240, doi: 10.1002/hyp.10594, 2015.
- 83 Botter, G., Bertuzzo, E., and Rinaldo, A.: Transport in the hydrologic response: Travel time distributions, soil moisture
84 dynamics, and the old water paradox, *Water Resources Research*, 46, W03514, doi:10.1029/2009WR008371, 2010.
- 85 Carey, S., and Woo, M.: Freezing of Subarctic Hillslopes, Wolf Creek Basin, Yukon, Canada. *Arctic, Antarctic, and Alpine*
86 *Research*, 37(1), 1–10, doi: 10.1657/1523-0430(2005)037[0001:FOSHWC]2.0.CO;2, 2005.
- 87 Craig, H. and Gordon L. I.: Deuterium and oxygen 18 variations in the ocean and the marine atmosphere, in: *Stable Isotopes in*
88 *Oceanographic Studies and Paleotemperatures*, Consiglio nazionale delle ricerche, Laboratorio di geologia nucleare, Pisa.
89 1965.
- 90 Dee, D.P., Uppala, S.M., Simmons, A.J., Berrisford, P., Poli, P., Kobayashi, S., Andrae U., Balmaseda, A.M., Balsamo, G.,
91 Bauer, P., Bechtold, P., Beljaars, A.C.M., van de Berg, L., Bidlot, J., Bormann, N., Delsol, C., Dragani, R., Fuentes, M.,
92 Geer, A.J., Haimberger, L., Healy, S.B., Hersbach, H., Hólm, E.V., Isaksen, L., Kållberg, P., Köhler, M., Matricardi, M.,
93 McNally, A.P., Monge-Sanz, B.M., Morcrette, J.J., Park, B.K., Peubey, C., de Rosnay, P., Tavolato, C., Thépaut, J.N., and
94 Vitart, F.: The ERA-Interim reanalysis: configuration and performance of the data assimilation system, *Quarterly Journal of*
95 *the Royal Meteorological Society*, 137(565), 553–597, doi: 10.1002/qj.828, 2011
- 96 Fatichi, S., Pappas, C., and Ivanov, V.Y.: Modeling plant-water interactions: an ecohydrological overview from the call to the
97 global scale, *WIREs Water*, 3, 327–368, doi: 10.1002/wat2.1125, 2016.
- 98 Filippa, G., Maggioni, M., Zanini, E., and Freppaz, M.: Analysis of continuous snow temperature profiles from automatic
99 weather stations in Aosta Valley (NW Italy): Uncertainties and applications, *Cold Regions Science and Technology*, 104–
00 105: 54–62, doi: 10.1016/j.coldregions.2014.04.008, 2014.
- 01 Gray, D.H.M., Male, D.H.: Snowcover ablation and runoff, in *Handbook of snow*. Pergamon Press. 1981.



- 02 Guttorp, P., and Xu, J.: (2011) Climate change, trends in extremes, and model assessment for a long temperature time series from
03 Sweden, *Environmetrics*, 22, 456–463, doi:10.1002/env.1099, 2011.
- 04 Harman, C. J.: Time-variable transit time distributions and transport: Theory and application to storage-dependent transport of
05 chloride in a watershed, *Water Resources Research*, 51, 1–30, doi:10.1002/2014WR015707, 2015.
- 06 Jansson, P.E.: SOIL model User's Manual: Second Edition. Swedish University of Agricultural Sciences, Department of Soil
07 Sciences, Division of Agricultural Hydrotechnics, 1998.
- 08 Jumikis, A. R.: *Thermal Geotechnics*. New Brunswick, N.J.: Rutgers University Press. 375 pp., 1977.
- 09 Karlsen, R. H., Seibert, J., Grabs, T., Laudon, H., Blomkvist, P., and Bishop, K.: The assumption of uniform specific discharge:
10 unsafe at any time? *Hydrol. Process.*, 30, 3978–3988, doi: 10.1002/hyp.10877, 2016a.
- 11 Karlsen, R. H., Grabs, T., Bishop, K., Buffam, I., Laudon, H., and Seibert, J.: Landscape controls on spatiotemporal discharge
12 variability in a boreal catchment, *Water Resour. Res.*, 52, 6541–6556, doi: 10.1002/2016WR019186, 2016b.
- 13 Kundzewicz Z.W, Mata, L.J., Arnell, N.W., Döll, P., Kabat, P., Jiménez, B., Miller, K.A., Oki, T., Sen, Z., and Shiklomanov,
14 I.A.: Freshwater resources and their management, In *Climate change 2007: impacts, adaptation and vulnerability*.
15 Contribution of Working Group II to the Fourth Assessment Report of the Intergovernmental Panel on Climate Change,
16 editor, Parry, M.L., Canziani, O.F., Palutikof J.P., van der Linden, P.J., Hanson C.E., Cambridge University Press:
17 Cambridge, UK; 173–210, 2007.
- 18 Kuppel, S., Tetzlaff, D., Maneta, M.P., and Soulsby, C.: ECH2O-iso 1.0: water isotopes and age tracking in a process-based,
19 distributed ecohydrological model, *Geosci. Model Dev.*, 11, 3045–3069, doi: 10.5194/gmd-11-3045-2018, 2018a.
- 20 Kuppel, S., Tetzlaff, D., Maneta, M.P., and Soulsby, C.: What can we learn from multi-data calibration of a process-based eco-
21 hydrological model?, *Environ. Model. Softw.*, 101, 301–316, doi:10.1016/j.envsoft.2018.01.001, 2018b.
- 22 Kurylyk, B. and Hayashi, M.: Improved Stefan Equation Correction Factors to Accommodate Sensible Heat Storage during Soil
23 Freezing or Thawing, *Permafrost and Periglacial Processes*, 27, 189–203, doi: 10.1002/ppp.1865, 2016.
- 24 Laudon, H., Sjöblom, V., Buffam, I., Seibert, J., and Mörth, M.: The role of catchment scale and landscape characteristics for
25 runoff generation of boreal streams, *Journal of Hydrology*, 344(3–4), 198–209, doi: 10.1016/j.jhydrol.2007.07.010, 2007.
- 26 Laudon, H., Taberman, I., Ågren, A., Futter, M., Ottosson-Löfvenius, M., and Bishop, K.: The Krycklan Catchment Study—A
27 flagship infrastructure for hydrology, biogeochemistry, and climate research in the boreal landscape, *Water Resour. Res.*, 49,
28 7154–7158, doi: 10.1002/wrcr.20520, 2013.
- 29 Laudon, H., and Ottosson Löfvenius, M.: Adding snow to the picture – providing complementary winter precipitation data to the
30 Krycklan Catchment Study database, *Hydrol. Process.*, 30, 2413–2416, doi: 10.1002/hyp.10753, 2016.
- 31 Laudon, H., Spence, C., Buttle, J., Carey, S.K., McDonnell, J.J., McNamara, J.P., Soulsby, C., and Tetzlaff, D.: Save northern
32 high-latitude catchments, *Nature Geoscience*, 10, 324–325, 2018.
- 33 Lee, T. J. and Pielke, R. A.: Estimating the soil surface specific humidity, *J. Appl. Meteorol.*, 31, 480–484, 1992.
- 34 Lindström, G., Bishop, K., and Ottosson Löfvenius, M.: Soil frost and runoff at Svartberget, northern Sweden—measurements
35 and model analysis, *Hydrological Processes*, 16, 3379–3392, doi: 10.1002/hyp.1106, 2002.
- 36 Liu, X, Sun, G., Mitra, B., Noormets, A., Gavazzi, M.J., Domec, J.-C., Hallema, D.W., Li, J., Fang, Y., King, J.S., and McNulty,
37 S.G.: Drought and thinning have limited impacts on evapotranspiration in a T managed pine plantation on the southeastern
38 United States coastal plain, *Agricultural and Forest Meteorology*, 262, 14–23, doi:10.1016/j.agrformet.2018.06.025, 2018.
- 39 Maneta, M. P. and Silverman, N. L.: A spatially distributed model to simulate water, energy, and vegetation dynamics using
40 information from regional climate models, *Earth Interact.*, 17, 1–44, 2013.



- 41 Maxwell, R.M., Condon, L.E., Danesh-Yazdi, M., and Bearup, L.A.: Exploring source water mixing and transient residence time
42 distributions of outflow and evapotranspiration with an integrated hydrologic model and lagrangian partial tracking
43 approach, *Ecohydrology*, 12, e2042, doi:10.1002/eco.2042, 2019.
- 44 McKay, M., Beckman, R., and Conover, W.: A Comparison of Three Methods for Selecting Values of Input Variables in the
45 Analysis of Output from a Computer Code, *Technometrics*, 21(2), 239-245, doi:10.2307/1268522, 1979.
- 46 Meløysund, V., Leira, B., Høiseith, K.V., and Lisø, K.R.: Predicting snow density using meteorological data. *Meteorological
47 Applications*, 14, 413-423, doi: 10.1002/met.40, 2007
- 48 Pearson, R.G., Phillips, S.J., Loranty, M.M., Beck, P.S.A., Damoulas, T., Knight, S.J., and Goetz, S.J.: Shifts in Arctic
49 vegetation and associated feedbacks under climate change, *Nature Climate Change*, 3, 673-677, 2013.
- 50 Peralta-Tapia, A., Soulsby, C., Tetzlaff, D., Sponseller, R., Bishop, K., and Laudon, H.: Hydroclimatic influences on non-
51 stationary transit time distributions in a boreal headwater catchment, *Journal of Hydrology*, 543, 7-16, doi:
52 10.1016/j.jhydrol.2016.01.079, 2016.
- 53 Piovano, T., Tetzlaff, D., Ala-aho, P., Buttle, J., Mitchell, C.P.J., and Soulsby, C.: Testing a spatially distributed tracer-aided
54 runoff model in a snow-influenced catchment: Effects of multicriteria calibration on streamwater ages, *Hydrological
55 Processes*, 32, 3089-3107, doi:10.1002/hyp.13238, 2018.
- 56 Pomeroy, J., Gray, D.M., Brown, T., Hedstrom, N.R., Quinton, W.L., Granger, R.J., and Carey, S.K.: The cold regions
57 hydrological model: a platform for basing process representation and model structure on physical evidence, *Hydrological
58 Processes*, 21, 2650-2667, doi: 10.1002/hyp.6787, 2007.
- 59 Riche, R. and Schneebeli, M.: Thermal conductivity of snow measured by three independent methods and anisotropy
60 considerations, *The Cryosphere*, 7, 217-227, doi:10.5194/tc-7-217-2013, 2013.
- 61 Schlesinger, W.H., and Jasechko, S.: Transpiration in the global water cycle, *Agricultural and Forest Meteorology*, 189-190,
62 115-117, doi: 10.1016/j.agrformet.2014.01.011, 2014.
- 63 Soheir, H., Farges, J-L., and Piet-Lahanier, H.: Improvement of the Representativity of the Morris Method for Air-Launch-to-
64 Orbit Separation, *IFAC Proceedings Volumes*, 47(3), 7954-7959, doi: 10.3182/20140824-6-ZA-1003.01968, 2014.
- 65 Schöne, B.R., Dunca, E., Mutvei, H., and Norlund, U.: A 217-year record of summer air temperature reconstructed from
66 freshwater pearl mussels (*M. margaritifera*, Sweden), *Quaternary Science Reviews*, 23(16-17), 1803-1816, doi:
67 10.1016/j.quascirev.2004.02.017, 2004.
- 68 Sprenger, M., Tetzlaff, D., Buttle, J., Laudon, H., and Soulsby, C.: Water ages in the critical zone of long-term experimental sites
69 in northern latitudes, *Hydrology and Earth System Sciences*, 22, 3965-3981, doi:10.5194/hess-22-3965-2018, 2018a
- 70 Sprenger, M., Tetzlaff, D., Buttle, J., Carey, S.K., McNamara, J.P., Laudon, H., Shatilla, N.J., and Soulsby, C.: Storage, mixing
71 and fluxes of water in the critical zone across northern environments inferred by stable isotopes of soil water, *Hydrological
72 Processes*, 32(12), 1720-1737, doi: 10.1002/hyp.13135, 2018b.
- 73 Stadnyk T., Delavau, C., Kouwen, N., Edwards, T.W.D.: Towards hydrological model calibration and validation: simulation of
74 stable water isotopes using the isoWATFLOOD model, *Hydrological Processes*, 27(25), 3791-3810, 2013.
- 75 Sterte, E.J., Johansson, E., Sjöberg, Y., Karlsen, R.H., and Laudon, H.: Groundwater-surface water interactions across scales in a
76 boreal landscape investigated using a numerical modelling approach, *Journal of Hydrology*, 560, 184-201,
77 doi:10.1016/j.jhydrol.2018.03.011, 2018.
- 78 Sturm, M., Taras, B., Liston, G.E., Derksen, C., Jonas, T., and Lea, J.: Estimating Snow Water Equivalent Using Snow Depth
79 Data and Climate Classes, *Journal of Hydrometeorology*, 11, 1380-1394, doi:10.1175/2010JHM1202.1, 2010.



- 80 Tetzlaff, D., Buttle, J., Carey, S. K., van Huijgevoort, M. H., Laudon, H., McNamara, J. P., Mitchell, C. P., Spence, C., Gabor, R.
81 S., and Soulsby, C.: A preliminary assessment of water partitioning and ecohydrological coupling in northern headwaters
82 using stable isotopes and conceptual runoff models, *Hydrological Processes*, 29(25), 5153-5173, 2015.
- 83 Tetzlaff, D., Piovano, T., Ala-Aho, P., Smith, A., Carey, S.K., Marsh, P., Wookey, P.A., Street, L.E., and Soulsby, C.: Using
84 stable isotopes to estimate travel times in a data-sparse Arctic catchment: Challenges and possible solutions, *Hydrological
85 Processes*, 32(12), 1936-1952, doi: 10.1002/hyp.13146, 2018.
- 86 US Army Corps of Engineers, North Pacific Division: Snow Hydrology; Summary Report of the Snow Investigation, Portland,
87 Oregon, 1956
- 88 van Huijgevoort, M.H.J, Tetzlaff, D., Sutanudjaja, E.H., and Soulsby, C.: Using high resolution tracer data to constrain water
89 storage, flux and age estimates in a spatially distributed rainfall-runoff model, *Hydrological Processes*, 30, 4761-4778, doi:
90 10.1002/hyp.10902, 2016.
- 91 Venäläinen, A., Tuomenvirta, H., Heikinheimo, M., Kellomäki, S., Peltola, H., Strandman, H., and Väisänen, H.: Impact of
92 climate change on soil frost under snow cover in a forested landscape, *Climate Research*, 17, 63-72, 2001.
- 93 Vogt, H. J.: Isotopentrennung bei der Verdunstung von Wasser, Staatsexamensarbeit, Institut für Umweltphysik, Heidelberg,
94 Germany, 1976.
- 95 Waite, W., Gilbert, L., Winters, W., and Mason, D.: Estimating thermal diffusivity and specific heat from needle probe thermal
96 conductivity data, *Review of Scientific Instruments*, 77, doi:10.1063/1.2194481, 2006.
- 97 Woo, M.: Impacts of climate variability and change on Canadian wetlands, *Canadian Water Resources Journal*, 17(1), 63-69,
98 doi:10.4296/ cwrj1701063, 2013.
- 99 Xie, C., and Gough, W.A.: A Simple Thaw-Freezing Algorithm for a Multi-Layered Soil using the Stefan Equation, *Permafrost
00 and Periglacial Processes*, 24, 252-260, doi:10.1002/ppp.1770, 2013.
- 01



1 **Appendix A: Application of frozen ground conditions and other EcH2O-iso adaptations**

2 Using Eqns 1-3 and 5, soil frost was estimated with a step-wise process using each soil layer (Carey and Woo, 2005). At the
 3 beginning of each time-step, k_{fi} was estimated for each soil layer. With the thermal conductivity and the depth of frost in each
 4 layer (z_{fi} , and conversely unfrozen depth, Δx), the thermal resistance of each layer was estimated ($R = z_{fi}/k_{fi}$). The depth of
 5 frost in each layer has a maximum of the total depth of the layer. If the total resistance to freeze soil layer m is exceeded (i.e. $T_s >$
 6 $N(m) = \lambda\theta\Delta x(\sum_{j=1}^{m-1} R(j))$, Carey and Woo, 2005), the soil layer is completely frozen. If the total resistance is not exceeded
 7 then partial freezing/thawing of the soil layer occurs:

$$\Delta z_f = -k_f(m) \sum_{j=1}^{m-1} R(j) + \sqrt{k_f(m)^2 \left(\sum_{j=1}^{m-1} R(j) \right)^2 + \frac{2k_f(m)N}{\lambda\theta}} \quad \text{A.1}$$

8 where the sum of the terms $R(j)$ are the resistance of frozen soil layers up to the soil layer currently undergoing freezing, and Δz_f
 9 is the increase/decrease in the depth of frost. The process is repeated each day to estimate the increase (freezing) or decreasing
 10 (thawing) of the frost front.

11 The limitation of a single, non-depth dependent porosity and hydraulic conductivity in the model structure was modified as
 12 a minor model structure change by using a simple exponential function to decrease the soil porosity and hydraulic conductivity
 13 with depth, similar to the approach employed by Kuppel et al. (2018) for the rooting profile. Similar to the original model
 14 structure, the approach assumes that the soil properties are the same for all soil layers (3), while increased consolidation of soils
 15 at deeper depths result in lower porosity and lower hydraulic conductivity. The porosity is estimated for layer 1 as:

$$\phi_1 = k \cdot \phi \cdot \left(1 - \exp\left(-\frac{d_1}{k}\right) \right) / d_1 \quad \text{A.2}$$

16 where d_1 is the soil depth of layer 1, ϕ_0 is the porosity at the soil surface, and k is the exponential rate of change of the porosity.

17 For layer 2:

$$\phi_2 = k \cdot \phi \cdot \left(\exp\left(-\frac{d_1}{k}\right) - \exp\left(-\frac{(d_1 + d_2)}{k}\right) \right) / d_2 \quad \text{A.3}$$

18 where d_2 is the depth of layer 2, and for layer 3:

$$\phi_3 = k \cdot \phi \cdot \left(\exp\left(-\frac{d_1 + d_2}{k}\right) - \exp\left(-\frac{d}{k}\right) \right) / (d_1 + d_2) \quad \text{A.4}$$

19 where d is the total depth of the soil, the sum of all soil layer depths. Equations A.2-A.4 can also be used to solve for the
 20 hydraulic conductivity in each soil layer (replace ϕ with K_h in each equation). The parameterization of k for both the porosity and
 21 hydraulic conductivity with depth should be carefully chosen. Parameterization should always be checked to ensure that the
 22 porosity in layer 3 is greater than the residual soil moisture (θ_r) and the permanent wilting point (θ_w).

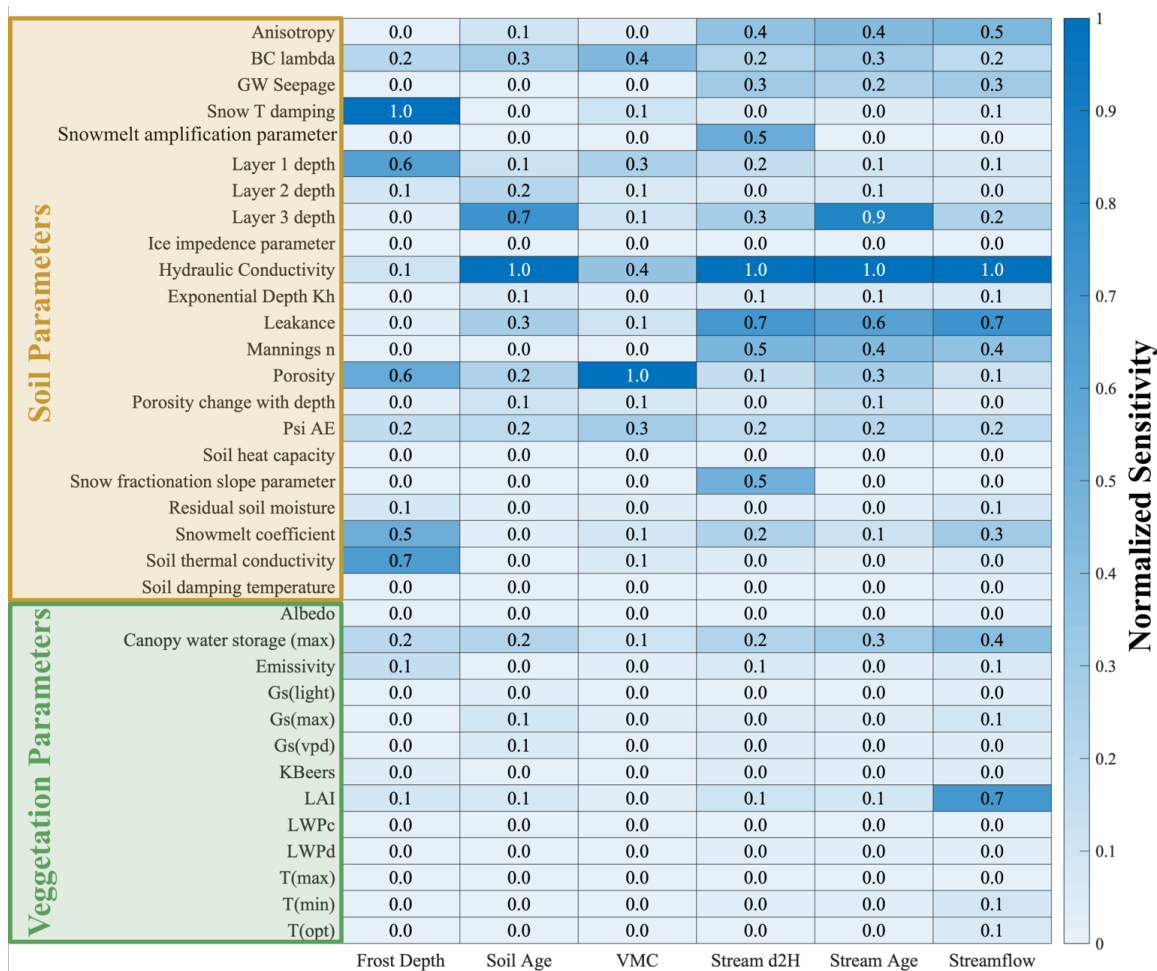
23

24 **Appendix B: Morris sensitivity analysis**

25 The aid with parameterization and reduce the total number of parameters used within calibration of the EcH2O-iso model, a
 26 sensitivity analysis with the Morris Sensitivity method and mean absolute error was used to assess how sensitive the model
 27 parameters were to stream discharge, stream isotopes ($\delta^2\text{H}$), and soil moisture (calibration time-series). Since the vegetation
 28 dynamics (carbon allocation mechanisms and vegetation growth) were not activated for the calibration, most vegetation
 29 parameters were not included in the sensitivity analysis as they would not result in any changes to observable metrics. These



30 parameters include: leaf allocation parameters, canopy quantum efficiency parameters, cold stress, and moisture stress leaf
 31 turnover parameters. Parameter sensitivity was assessed using the radial step method and 50 different trajectories. Initial
 32 parameterizations were established using Latin Hypercube Sampling (LHS) to maximize the distance between the randomized
 33 trajectories. Each radial step deviated from the initial parameterization by progressively changing each parameter by half of the
 34 parameters range. For example, initial parameter value of 0.1 with a range of 2 (0 – 2) results in a new parameter value of 1.1
 35 (0.1 + (2-0)/2). The sensitivity of the parameter was assessed against the original parameterization for the trajectory using the
 36 mean absolute error.



37
 38 **Figure B.1: Normalized mean absolute error for each time-series. Values of 1 indicate the most sensitive parameters and 0 indicates**
 39 **the least sensitive parameters. Additional information on the naming convention is found at [iso.readthedocs.io/en/latest/Setup.html](https://ech20-

 40 <a href=)**

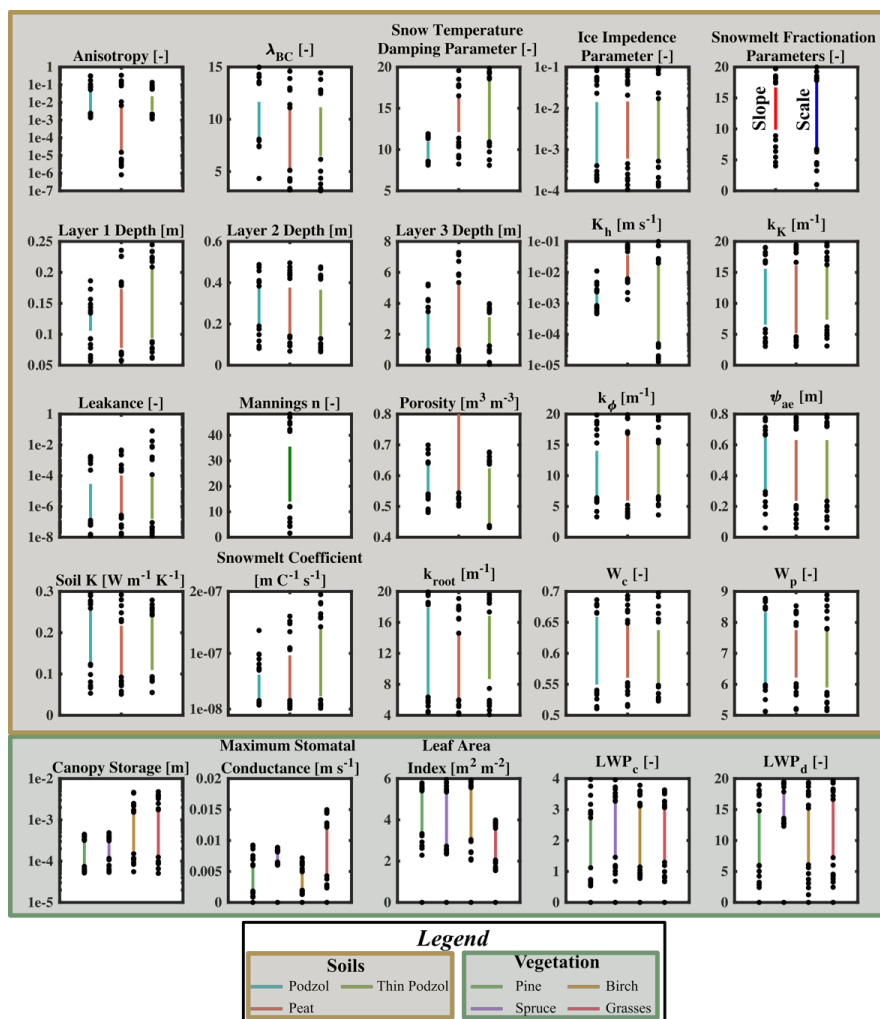
41 Mean absolute error was averaged for all trajectories to determine the mean sensitivity of each parameter. For streamflow, the
 42 parameters most sensitive are a mixture of soil parameters (e.g. hydraulic conductivity, snowmelt coefficient, and anisotropy),
 43 channel parameters (e.g. Mannings n and leakance), and vegetation parameters (e.g. leaf area index and canopy water storage).
 44 Stream isotopes are similarly affected by soil and stream parameters, and show significant influence of the newly introduced



45 snowmelt fractionation parameters (slope and amplification parameters). As anticipated, soil moisture simulations are most
46 sensitive to soil parameters, with the most sensitivity related to the porosity. The parameter sensitivity of frost depth was also
47 tested due to the newly implemented frost module. The frost depth was most sensitive to the snow temperature damping
48 parameter, with other sensitivity related to winter and thermal processes (snowmelt coefficient and soil thermal conductivity).
49 Since it is not possible to directly calibrate the soil water or streamflow water ages, the sensitivity analysis was evaluated to
50 provide additional assessment of which parameterizations will result in changes and uncertainties of the water ages. Except for
51 the soil heat capacity (set to $2.205 \times 10^6 \text{ W kg}^{-1} \text{ C}^{-1}$), residual soil moisture (set to 0.05), and the temperature at the damping depth
52 (set to 5°C), all other soil parameters (Fig B.1) were used in calibration since they showed to be sensitive for the calibration time-
53 series. Vegetation parameters used in calibration included the canopy water storage, leaf area index, maximum stomatal
54 conductance ($G_{s,\max}$) and two soil-based vegetation parameters controlling the sensitivity of vegetation to suction potential and
55 moisture content.

56 ***Appendix C: Model calibration parameters***

57 Model calibration showed a reduction in the parameter space for almost all parameters, where the maximum range of parameters
58 is shown with the upper and lower bounds of the plots (Fig C.1). Differences between parameterization of soils was most
59 noticeable for anisotropy, hydraulic conductivity (K_h) and porosity (ϕ), while for vegetation, canopy storage, maximum stomatal
60 conductance ($G_{s,\max}$) and leaf area index (LAI) varied most between the vegetation types.

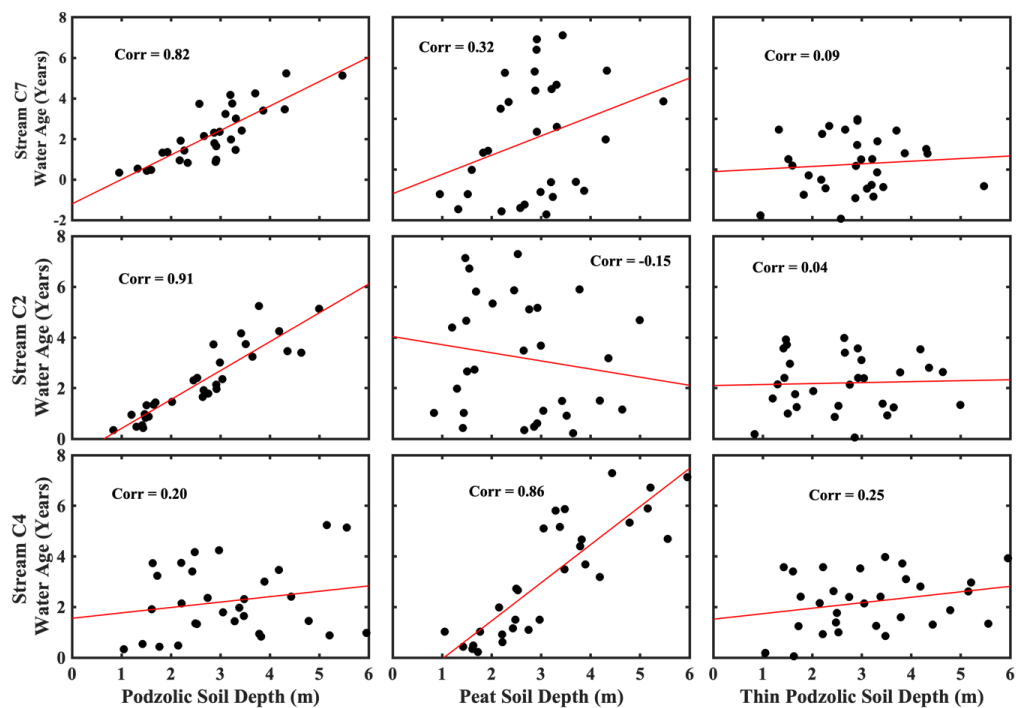


61

62 **Figure C.1: Calibration parameterization for soil and vegetation parameters for each soil and vegetation type. Lines represent the 25-**
 63 **75th quantiles and circles are outliers for the quartiles.**

64 **Appendix D: Simulated layer depth vs. stream water ages**

65 Stream water ages were expected to be predominantly controlled by the depth of the third soil layer in each of the soil types (Fig
 66 B.1). The relatively old stream water ages observed within the simulations were on the upper end of the previously simulated
 67 water ages, with median ages of ~3 years for all streams. A direct correlation was observed for each stream to the depth of the
 68 dominant soil type of the sub-catchment. The overall catchment outlet (C7) was dominated by podzolic soils, and showed a
 69 strong (0.82 correlation coefficient) 1:1 relationship with a regression of the stream water age to the depth of the soil water (1
 70 year of stream age for each meter of soil depth) (Fig D.1). A similar, stronger, 1:1 relationship of stream water age to soil depth
 71 was observed at the outlet of sub-catchment C2, which was also dominated by podzolic soils (Fig D.1). Unsurprisingly, in the
 72 peat dominated C4 catchment, a strong relationship (0.86 correlation coefficient) was observed between the peat soil depth and
 73 stream water age; however, the stream water became older with soil depth than in the podzolic soil dominated catchments.



74

75

Figure D.1: Linear regression and correlation coefficients for stream water age at each sub-catchment against the soil depth